Quasistatic and continuous dynamic characterization of the mechanical properties of silk from the cobweb of the black widow spider *Latrodectus hesperus*

Todd A. Blackledge[1],*, John E. Swindeman[2] and Cheryl Y. Hayashi[1]

[1]*Department of Biology, University of California, Riverside, CA 92521, USA* and [2]*MTS Systems Corporation, 1001 Larson Drive, Oak Ridge, TN 37830, USA*

*Author for correspondence at present address: Department of Biology, University of Akron, Arkon, OH 44325-3908, USA (e-mail: blackledge@uakron.edu)

Summary

Spider silks are among the strongest and toughest known materials, but investigation of these remarkable properties has been confined largely to orb-weaving spiders. We investigated the mechanical performance of silk from the cobweb-weaving spider *Latrodectus hesperus*. Both silk from the scaffolding region of the web and sticky gumfooted capture lines had material properties similar to the major ampullate silk that orb weavers use as the framework for their orb webs. Major ampullate fibers obtained from anaesthetized *Latrodectus* spiders were similar, but exhibited increased stiffness and reduced extensibility. Novel continuous dynamic analysis of the silks revealed that the loss tangent (tanδ) increased rapidly during the first 2–3% of extension and reached a maximum near the yield point of fibers. The loss tangent then rapidly declined at an ever-decreasing rate until failure. We suggest that these data support molecular models for the mechanics of spider silk. We also demonstrate that the addition of sticky aggregate glue to the ends of the gumfooted lines modulates their mechanical performance – reducing stiffness and increasing extensibility. The storage modulus of viscid regions of the gumfooted lines was much lower than dry regions. This may be explained by disruption of hydrogen bonding within the amorphous regions of the fibers due to hydration from the glue.

Key words: biomechanics, continuous dynamic analysis (CDA), dynamic mechanical analysis (DMA), spider web, major ampullate silk, polymer, Theridiidae, loss tangent, viscoelasticity.

Introduction

The beauty of the intricate shapes of spider webs fascinates people, but webs offer more than aesthetic appeal for biological research. The silk fibers used to construct webs have long been a favorite topic of study for materials scientists because some spider silks are among the toughest known materials (Gosline et al., 1986). However, almost all research on spider silk mechanics has been conducted upon silks spun by only a few species of spiders, all of which construct similar types of orb webs. Orb webs, flat wheel-shaped aerial nets, are remarkable architectural structures that function to arrest and absorb the kinetic energy of flying insect prey. It is this selective pressure that is hypothesized to have influenced the material properties of the silks used to construct orb webs (Gosline et al., 1986; Opell and Bond, 2001).

Modern phylogenetic studies have demonstrated that the orb web is an intermediate, rather than a highly derived, architecture within the diversification of spider webs (Coddington and Levi, 1991; Griswold et al., 1998). For example, spiders in the Theridiidae spin cobwebs. Because theridiids have orb web weaving ancestors, this implies that the seemingly chaotic architecture of the cobweb originated from the highly stereotyped orb architecture (Agnarsson, 2004; Coddington, 1986, 1990; Griswold et al., 1998). At first glance, cobwebs appear to be disorganized tangles of silk. However, cobwebs possess suites of discrete architectural elements that are common to webs constructed by different species and even different genera of theridiid spiders (Agnarsson, 2004; Benjamin and Zschokke, 2002, 2003; Coddington, 1986).

Latrodectine spiders constitute a basal clade within the Theridiidae and their cobwebs potentially represent an ancestral architecture for the family (Agnarsson, 2004; Arnedo et al., 2004; Benjamin and Zschokke, 2002). These '*Latrodectus*-type' webs consist of a retreat that is either suspended within the web or at the web periphery, a supporting structure of dry silk that includes both a sheet of radiating threads and peripheral support threads that suspend the web in space, and sticky gumfooted lines that attach to the substrate and function as the primary capture elements of the web (Fig. 1; Benjamin and Zschokke, 2002, 2003). Cobwebs are highly three-dimensional and lack viscid capture spirals, in

contrast to ancestral orb webs. The construction of cobwebs is also less stereotyped and cobwebs are continuously added to over many days, in contrast to orb webs, which are completed in a single bout of construction. Furthermore, cobwebs generally capture pedestrian rather than aerial prey (Hodar and Sanchez-Pinero, 2002). Thus, theridiid spiders use silks in a very different ecological context than did their orb-weaving ancestors. Yet, relatively little is known about the mechanical properties of cobweb silks.

We chose to investigate the web silks spun by the western black widow *Latrodectus hesperus* to construct cobwebs. In this study, we compare the mechanical properties of silks from the two primary architectural regions of the web, the sheet and gumfooted threads, as well as silk obtained from the major ampullate gland of anaesthetized spiders. We discuss the glandular origin of web elements, compare the mechanics of cobweb silks to orb webs, and provide novel data on the dynamic material properties of spider silk.

Materials and methods
Care of spiders

Seven female western black widows, *Latrodectus hesperus* Chamberlin and Ivie 1935, were collected from Riverside, California during Summer and Fall 2003. Spiders were maintained in the laboratory in $37 \times 22 \times 24$ cm plastic terraria and fed a diet of crickets (*Acheta domesticus*). We provided cardboard shelters as substrates for the spiders to construct webs. The shelters consisted of two separate portions placed adjacent to one another. The retreat portion was a simple box, open on one end, with a small roll of paper in an upper corner that encouraged widows to construct the retreat portions of their webs. The second half of the shelter consisted of a roof and floor of cardboard held together by three cardboard pillars. This allowed the spiders to construct the capture sheet portion of webs in structures that could be removed from the terraria, providing us easy access to the scaffolding and gumfoot silk while the spider remained in its retreat. All spiders were adult or penultimate females and varied in weight from 0.09–0.82 g, for penultimate and gravid females, respectively.

Collection of silk

We collected three different types of silk samples from each of the seven spiders. Scaffolding silk and gumfooted lines were collected directly from webs onto 'c' shaped cardboard mounts. The 10 mm gap between the arms of the card set a standard gage length. Both arms of the 'c' were first coated with small amounts of cyanoacrylate glue (Superglue™). The cards were then adhered to silk strands in the appropriate portion of the web. Finally, a hot wire was used to cut the silk on either side of the mount, freeing the silk thread from the web without altering the tension of the sample. We also obtained major ampullate silk directly from spiders through forcible silking (Work, 1976). Spiders were first removed from webs and anaesthetized with CO_2 for 2–5 min. We then restrained the unconscious spiders, ventral side facing up, onto

a petri dish using transparent tape such that the spinnerets of the spider were accessible. The petri dish was then placed on the stage of a stereomicroscope and the spinneret region was illuminated with fiber optic lights. Thus, we could see the fibers emanating from the major ampullate spigots while we manually pulled fibers from the spider. This allowed us to be certain of the glandular origin of the fibers. These forcibly silked threads were taped to cardboard mounts across 21 mm diameter gaps. Samples were then securely affixed to the mounts, at both edges of the 21 mm gap, using cyanoacrylate glue. We collected a total of six to nine samples of each type of silk – scaffolding, gumfoot, and manually pulled (i.e. forcibly silked) major ampullate silk, for each of the seven black widow spiders.

For 21 of the gumfooted lines sampled, we also collected a second sample from the glue-coated 'foot' portion of the line, which is covered with a viscid aggregate gland secretion that adheres to prey. Aggregate glue plays an essential role in the mechanical performance of orb weaver capture silk (Vollrath and Edmonds, 1989) and this sampling protocol allowed us to test the effects of theridiid glue secretions on silk mechanics.

All samples were collected within the first 5–14 days after spiders were brought into the lab, and typically all three types of silk from an individual spider were collected and tested on the same day. Mechanical tests were performed at a temperature of 21–23°C and ambient humidity during testing was usually 25–40%, but was as high as 70% for one of the spiders.

We used polarized light microscopy to obtain three digital images of the silk fibers within each sample, except for the glue-coated portions of the gumfooted lines, and then measured the diameters of the fibers using NIH Image 1.63 (US National Institutes of Health). These diameters were then used to calculate the cross-sectional area of each sample being tested. This method produces highly repeatable measurements that are similar in accuracy to measurements obtained through scanning electron microscopy, but also accounts for variation in cross-sectional area from sample to sample (Blackledge et al., 2005a).

Quasistatic mechanical analysis

Load-extension data were generated using a Nano Bionix tensile tester (MTS Systems Corp., Oak Ridge, TN, USA). The Nano Bionix is capable of generating load-extension data from very fine silk fibers, with a load resolution of 50 nN and an extension resolution of 35 nm. All fibers were extended at a constant rate of 1% strain s⁻¹ until the fibers failed. This strain rate was chosen because it was within the range of many other studies on spider silk mechanics, maximizing comparability of results. Raw load–extension data were then transformed into stress and strain values to normalize data across samples of silk of different sizes. Stress measures the force per cross-sectional area applied to a fiber, allowing comparison of the relative load applied to fibers of different diameters. We chose to calculate true stress (σ_{tr}), where load is normalized to the instantaneous cross-sectional area of fibers, as:
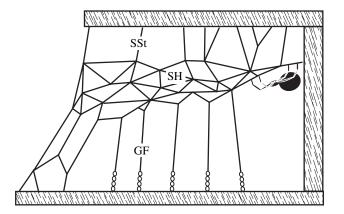
Fig. 1. Western black widows (*Latrodectus hesperus*) construct cobwebs that consist of three primary regions. A supporting structure (SSt) of dragline threads is used to suspend a non-sticky sheet (SH) that the spider uses to move around the web. Gumfooted lines (GF) extend downward from the sheet to the substrate and are held under tension by the sheet.

$$\sigma_{tr} = F/A \; , \qquad (1)$$

where F is the force applied to the specimen and A is the estimated cross-sectional area of the specimen calculated from the original cross-sectional area under an assumption of constant volume. Ideally, true stress would be calculated using the actual cross-sectional area of the specimen measured at each extension value. However, it is technologically difficult to visualize fiber diameters during stress-strain tests such that the cross-sectional area is typically calculated from the original cross-sectional area using an assumption of constant volume. Currently there are few data on whether or not this assumption is valid for spider silks.

Our use of true stress is distinct from much of the literature on spider silk mechanics, which often uses engineering stress where force measurements at all extension values are normalized to the initial cross-sectional areas of fibers. Our use of true stress rather than engineering stress generates more realistic values of the stress experienced by highly extensible fibers, such as spider silk. Furthermore, true stress values facilitate comparison of the mechanical properties of different kinds of silks that may vary widely in their extensibilities, and an important long-term goal of our research program is to generate comparative data on a broad range of silks spun by taxonomically diverse spiders.

Strain measures the extension of a fiber relative to its length and we again chose to use true strain rather than engineering strain values. True strain (ε_{tr}) was calculated as:

$$\varepsilon_{tr} = \log_e (L/L_o) \; , \qquad (2)$$

where L is the instantaneous length of the fiber at each extension value and L_o is the original gage length of the fiber. Again, true strain provides a more realistic measure of the stretchiness of highly extensible fibers, such as spider silk.

We then used true stress and true strain measurements to calculate five variables of interest. Young's modulus measures
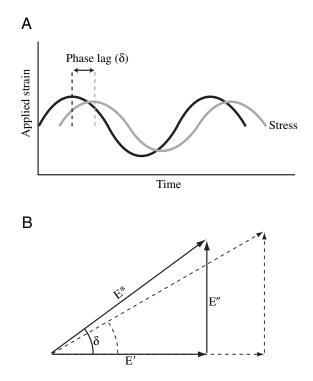

Fig. 2. Dynamic analysis of mechanical behavior quantifies the elastic and viscous behavior of materials. (A) The phase lag (δ) is the displacement of the sinusoidal stress response (gray) to a tiny applied strain oscillation (black). The degree to which the peak amplitude of the stress response curve is in phase with that of the applied strain oscillation measures elasticity while the viscosity is measured by the degree to which the stress response 90° out of phase with strain. (B) Vector relationship between dynamic material properties are illustrated by the solid line vectors. Dynamic stiffness (E^*) is determined by the storage modulus (E') and the loss modulus (E''). Tanδ (loss tangent) defines the relative viscous and elastic behavior of the material. E' and E'' can change independently of one another and of tanδ. The dotted line vectors illustrate an example where increases in both E' and E'' result in a decrease in tanδ.

the stiffness, or ability of fibers to resist deformation, and is calculated as the slope of the linear region of the stress-strain curve prior to the yield point. The yield strain measures the point at which the mechanical behavior of fibers changes from elastic to viscous. Extensibility is the true strain at the point of failure of the fiber. Ultimate strength is the true stress at the point of failure of the fiber. Toughness (i.e. work of extension or work to fracture) is a measure of the energy necessary to rupture a fiber of a given volume and was calculated as the area under the 'true stress–true strain' curve.

Continuous dynamic analysis

Traditional quasistatic tensile tests provide a measure of how much energy is absorbed by fibers as they are extended (i.e. 'toughness' as delimited by the area under the stress–strain curve). Quasistatic analysis can measure stiffening of fibers as an increase in the rate of energy absorption, but it cannot determine how that energy is absorbed. For instance, a similar increase in the stiffness of a fiber can occur both through an
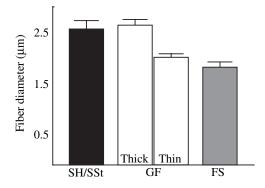
Fig. 3. Mean (±S.E.M.) diameter of single fibers from the sheet and supporting structure regions (SH/SSt; N=54), gumfooted lines (GF; N=36), and forcibly silked major ampullate fibers (FS; N=52). Diameters for the thicker and thinner pair of fibers at the base of gumfooted lines are shown separately.

increase in elastic effects such as crosslinking between silk fibroin molecules or through an increase in viscosity caused by friction between molecules. Dynamic analysis of material properties distinguishes itself from quasistatic analysis by measuring how much energy is absorbed through these viscous and elastic processes.

The Nano Bionix performs a novel continuous dynamic analysis (CDA) of silk mechanics. It does so by imposing a slight oscillating dynamic strain upon the silk fiber as it is extended. The Nano Bionix then measures the dynamic stress response to this oscillating strain. The degree to which the dynamic stress response is in phase with the dynamic strain oscillation provides a measure of the elastic behavior of the fiber (storage modulus) while the viscous behavior (loss modulus) is measured by the degree to which the oscillation in dynamic stress lags behind that of the dynamic strain. In Fig. 2A, the resulting dynamic stress is neither completely in phase with the dynamic strain (where the two sinusoidal curves would overlap perfectly, offset by 0°) nor completely out of phase (where the stress response would be 90° out of phase with the strain wave). Instead it exhibits viscoelastic behavior with a phase lag δ somewhere between 0° and 90°. The amplitude of the dynamic stress and the degree to which δ is in phase with the applied dynamic strain measures the elastic response, storage modulus (E'), and is affected by the absorption of energy through the reversible deformation of chemical bonds and breaking of ionic bonds within and between silk fibroins. The amplitude of the dynamic stress and the degree to which δ is out of phase with the applied dynamic strain measures the viscous response, loss modulus (E''), which is affected by the transformation of kinetic energy into heat due to friction within and between fibroins, as well as the permanent breaking of chemical bonds. A classic analogy to these two dynamic variables is that of a dropping ball. The height to which the ball bounces is proportional to its storage modulus while the difference between the height of the bounce and the height from which it was dropped is proportional to the loss modulus. Dynamic strain (ε_t) is calculated as:

$$\varepsilon_t = \varepsilon_o \sin(\omega t) , \qquad (3)$$

where ε_o is the dynamic strain amplitude, ω is the angular frequency, and t is time. Dynamic stress (σ_t) is calculated as:

$$\sigma_t = \sigma_o \sin(\omega t + \delta) , \qquad (4)$$

where σ_o is the dynamic stress amplitude, ω is the angular frequency, t is the time, and δ is the phase lag. The dynamic stiffness of the material (E^*) is defined as:

$$E^* = \sigma_o / \varepsilon_o . \qquad (5)$$

This allows the dynamic stress, σ_t, to be expressed as:

$$\sigma_t = \varepsilon_o E^* \sin(\omega t + \delta) , \qquad (6)$$

which can be rewritten as:

$$\sigma_t = \varepsilon_o (E^* \cos\delta)\sin(\omega t) + \varepsilon_o (E^* \sin\delta)\cos(\omega t) . \qquad (7)$$

The storage modulus (E') is $E^* \cos\delta$ while the loss modulus (E'') is $E^* \sin\delta$. Finally, the ratio of energy stored to energy lost, the loss tangent (tanδ), is calculated as:

$$\tan\delta = E'' / E' , \qquad (8)$$

where E'' is the loss modulus and E' is the storage modulus. It is important to note that the loss tangent (tanδ) can vary as a function of changes in how fibers store energy elastically, how fibers dissipate energy as heat, or both. In other words, an increase both in loss and in storage modulus can result in either a decrease or increase in the loss tangent (Fig. 2B).

CDA is distinguishable from more traditional dynamic mechanical analysis (DMA) of material properties because CDA measures storage and loss modulus as a continuous function of extension. In contrast, DMA measures storage and loss modulus at a constant extension but across a range of changes in oscillation frequencies or temperatures. DMA is performed at a constant static strain that is quite small, typically 1–2%, and usually within the elastic limit of polymers. However, spider silks can stretch well beyond this 1–2% during ecological function and their viscoelastic nature makes it likely that their mechanical behaviors would change as a function of extension such that spider silks would not display the same mechanical behavior at different strains. Thus, it is important to examine the mechanical behavior of silks across a wide variety of strains. For this study, we used a dynamic strain oscillation with a frequency of 20 Hz and dynamic force amplitude of 4.5 mN, resulting in a maximum dynamic displacement of 45 µm.

Statistical analysis

We used one-way analysis of variance (ANOVA) to compare thread diameter, Young's modulus, extensibility, ultimate strength, and toughness across the three types of silk that we sampled. We used linear regression to test for relationships between stress and strain within each type of silk, as well for relationships between cross-sectional area of fibers and each of the four quasistatic parameters that we measured. One-way ANOVAs were also used to compare the initial, final,

and maximum values of loss tangent, as well as loss tangent at the yield point and the true stress and true strain values at the maximum loss tangent across silk types.

Results

The diameters of individual threads varied significantly across the three types of silk (Fig. 3; one way ANOVA, $F_{2,181}$=12.6, $P<0.00001$). *Post hoc* comparisons using Tukey's HSD tests for unequal sam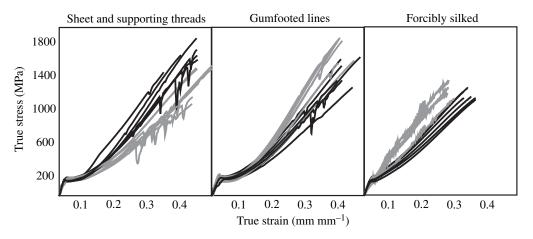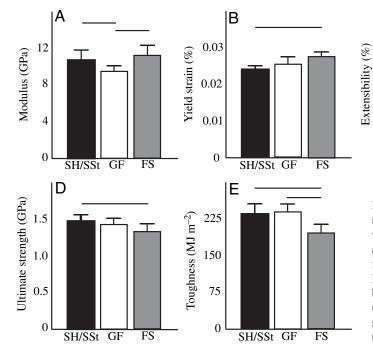ple sizes indicated that pulled major ampullate fibers were thinner than both scaffolding ($P<0.00005$) and gumfooted fibers ($P<0.01$). Sticky gumfooted lines were found to consist of four strands because spiders retrace their path during gumfoot construction (see below). One pair of threads from the sticky gumfooted lines was consistently larger in diameter than the other (Fig. 3). The diameters of individual threads from this larger pair were similar to the diameters of individual threads from the sheet/supporting structure of webs. The diameters of individual threads from the smaller thread pair were only marginally larger than those of pulled major ampullate silk (Fig. 3; t_{96}=2.1, $P<0.05$).

Quasistatic properties of silks

The stress-strain characteristics of all three types of silk were qualitatively similar. These included an initially stiff modulus

Fig. 4. Exemplar stress-strain curves for each type of silk. The gray and black lines denote test data for two different spiders (*N*=6 for each spider).

of 9–11 GPa for the first ~2% of strain. The fibers then reached a 'yield region' where mechanical behavior varied from only a slight strain softening (particularly for forcibly silked samples) to a distinct drop in stress. Subsequently, this yield region was followed by a strain hardening that was largely linear and continued until failure of the fiber (Fig. 4). Occasionally, sudden slight drops in stress were sometimes exhibited by fibers near failure (Fig. 4). The stress-strain curves quickly recovered to their previous stiffness after these drops. Furthermore, these drops only occurred when testing multistranded fibers. Therefore, we interpret them as areas where fibers were snapping around one another, suddenly loosening and then regaining stress. The mechanical properties of fibers exhibiting this 'noise' were not noticeably different from tests where these drops did not occur.
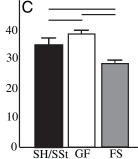

Fig. 5. Mean (±S.E.M.) material properties of *L. hesperus* silk from the sheet/supporting thread region (SH/SSt) of webs (*N*=54), gumfooted capture threads (GF; *N*=47), and single strands of major ampullate silk forcibly pulled from spinnerets of anesthetized spiders (FS; *N*=52). Horizontal bars denote significant pairwise differences between means using *post hoc* Tukey's HSD tests for unequal sample sizes. (A) Young's modulus; (B) yield strain; (C) extensibility; (D) ultimate strength; and (E) toughness.

Fig. 6. Relationship between extensibility and ultimate strength for sheet and supporting thread silk (*N*=54), gumfooted capture threads (*N*=47), and forcibly silked major ampullate threads (*N*=52). Correlation coefficients are from linear regression (*P*<0.05 for sheet/supporting threads and *P*<0.001 for gumfooted lines).

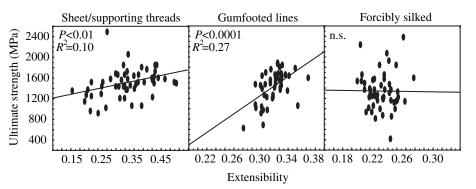There was significant variation among silk types for all five quasistatic mechanical parameters (Fig. 5; one-way ANOVAs, all *P*<0.05). Scaffolding silk was slightly stiffer and less extensible than gumfooted silk, but did not differ in ultimate strength or toughness. Forcibly silked major ampullate fibers exhibited greater differences from the other two types of silk. These fibers were less extensible and had lower toughness than gumfooted and scaffold silks. The modulus of forcibly silked major ampullate silk was also slightly higher than that for gumfooted silk and ultimate strength was lower than that for scaffold silk.

Extensibility and ultimate strength were positively associated with one another for both scaffold and gumfoot silk, but not for pulled major ampullate silk (Fig. 6). Variation in quasistatic mechanical properties of silk was largely independent of cross-sectional area, except for extensibility (Fig. 7). Thicker fibers had greater extensibility for both gumfooted and pulled major ampullate fibers (*P*<0.05). A similar positive, but non-significant trend was exhibited by the scaffold thread in relation to thread diameter.

Dynamic properties of silks

The storage modulus of all three types of silk changed in a non-linear fashion as fibers were strained (Fig. 8). Storage modulus was initially flat or decreased slightly to a low around the yield point of the fiber, before increasing in a relatively linear fashion as the fibers were subsequently strained to failure. In contrast, the loss modulus of all fibers increased sharply during the first 2–5% of strain, exhibited a rapid drop near the yield point, and then increased linearly at a lower slope until failure.

Pulled major ampullate fibers exhibited a higher storage modulus and a lower loss modulus than either scaffold or gumfoot silk. For all types of silk, loss modulus was approximately one order of magnitude less than storage modulus, resulting in loss tangent values that ranged from 0.03–0.07 initially and then increased to a maximum of 0.12–0.20 before decreasing again (Figs 8, 9). The dynamic behavior of scaffold and gumfooted threads was similar to one another, while pulled major ampullate silk differed significantly from both scaffold and gumfooted silks for all parameters except strain at maximum loss tangent (Tukey's HSD tests for unequal sample sizes, *P*<0.05). In particular, initial loss tangent was approximately 50% lower for pulled major ampullate silk.

Structure and properties of gumfooted lines

Gumfooted lines consisted of two pairs of fibers, one of which was approximately 25% thicker than the other (Fig. 3). Gumfooted lines were coated with aggregate glue secretions along their lower 5–10 mm and the thinner pair of fibers was joined to the thicker pair of fibers approximately 1–3 cm above this gluey foot (Fig. 10). This connection consisted of many fine fibers and the thinner pair of gumfooted fibers was cut just about this connection. The remaining portion of these thinner fibers could be seen curled up at the connection of the thicker fiber pair to the scaffolding of the web.

Two juvenile *L. hesperus* were observed while constructing gumfoots in the field (Riverside, CA, USA). In each instance, the spider rapidly descended to the substrate upon a dragline. The spider then turned around so that it was facing up toward the web and set an attachment to the substrate, while grasping the initial dragline in its front leg. Then it moved its spinnerets along the distal portion of the gumfoot, presumably laying the second fatter dragline and aggregate glue. With its hindleg still on the substrate, the spider briefly touched its chelicerae to the original dragline, cutting the original dragline. The spider then rapidly ascended the thread.

The gluey region of the gumfooted fiber had a greater extensibility, ultimate strength, and toughness relative to the adjacent region of dry gumfooted fiber (Fig. 11; paired *t*-tests, *t*=3.6–6.2, d.f.=20, *P*<0.0025–0.00001). Young's modulus was much lower (*t*=8.3, d.f.=20, *P*<0.000001) for the viscid region of the gumfooted thread. The dynamic characteristics of the viscid and dry portions of the gumfooted fibers differed most dramatically from one another during the first 20% of strain and then tended to converge with each other (Fig. 12). Storage modulus of the viscid portion of the fiber was initially four times lower than that of the dry portion and subsequently increased steadily rather than showing the drop in storage modulus over the first 2–3% of strain that characterized dry fibers. Loss modulus was similar between the wet and dry gumfooted samples, except within the initial elastic region. Dry portions of gumfooted fibers exhibited a rapid increase in loss modulus up to the yield point while wet portions had a higher initial loss modulus that resulted in a relatively linear increase in loss modulus throughout fiber extension.
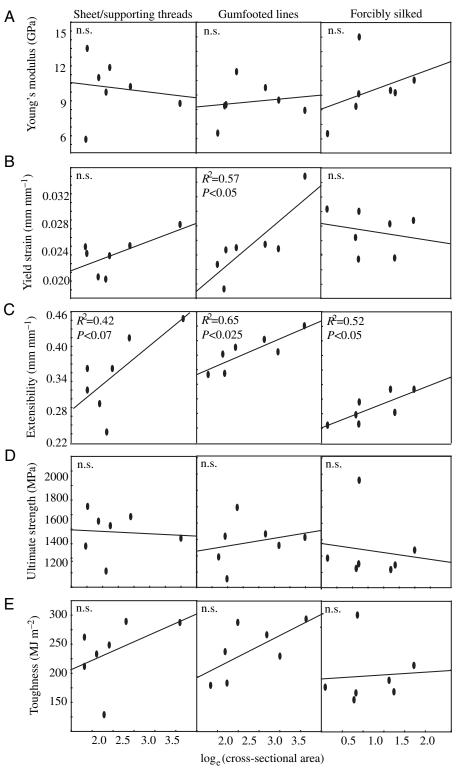
Fig. 7. Relationship between cross-sectional areas of silk threads and mechanical properties. Data are the means for each spider (*N*=7). Regressions of mechanical characteristics against cross-sectional area with significant correlation coefficients and *P*-values are indicated. (A) Young's modulus; (B) yield strain; (C) extensibility; (D) ultimate strength; and (E) toughness.

Discussion

The *L. hesperus* sheet/supporting threads, gumfooted lines, and forcibly silked major ampullate fibers all exhibited stress-strain behavior qualitatively similar to major ampullate silk from other spiders. Initially, stress increased rapidly in a linear relationship with strain until reaching a yield point. At the yield point, the mechanical behavior of silks varied from a pronounced decrease in stiffness for some tests to only a minor strain softening for other tests. The relationship between stress and strain was still positive after the yield point, but often somewhat nonlinear (Fig. 4). The mechanical performance of these black widow silks was also quantitatively similar to major ampullate silk spun by orb-weaving spiders and to Lawrence et al.'s (2004) study of *L. hesperus* major ampullate silk fibers that were obtained by dropping spiders through the air (Table 1).

Our mechanical data contrast with those obtained for scaffolding silk of *L. hesperus* webs by Moore and Tran (1999). They reported that silk from the sheet and supporting structure of *L. hesperus* webs was mechanically distinct from orb weaver major ampullate silk because it had a 'j' shaped stress-strain curve with an extremely high compliance over the first 3–5% of strain, rather than the high stiffness initially exhibited by orb weaver major ampullate silk (see Fig. 4). We never found silk with the initial high compliance behavior described by Moore and Tran (1999), despite sampling fibers from all regions of the cobwebs from the same species of spider from the same geographic region. Both studies tested silks of similar ages (3–14 days) and used similar strain rates (~1–2% s^{-1}) so that methodological differences *per se* seem unlikely to account for the discordance between our studies. Instead, one potential difference is in how we interpreted when fibers were fully tensed, which delimits the beginning of the tensile test (i.e. the zero point of strain). Moore and Tran's fibers may not have been fully tensed at the start of their data collection, such that the initial 5% of strain with high compliance in their study actually represented data taken from fibers that were only partially under tension. In fact, Moore and Tran's stress–strain curves qualitatively resemble those of our study, and most other mechanical analyses of major ampullate silk from orb-
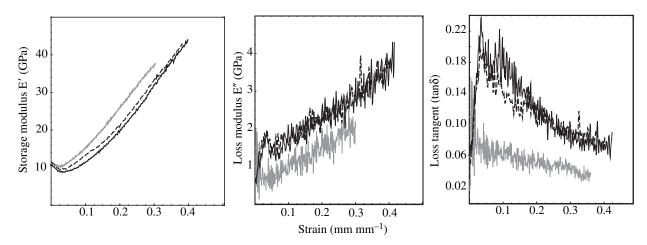
Fig. 8. Dynamic mechanical properties for black widow silk. Exemplar curves are shown for sheet/supporting threads (black), gumfooted lines (dotted), and forcibly silked major ampullate fibers (gray).

weaving spiders, if the tests began at '5% strain', where they seem to show the initially stiff elastic region that characterizes major ampullate silk.

Casem et al. (1999) also argued that *L. hesperus* scaffolding silk was a unique material. They found that silk collected directly from cobwebs had an amino acid composition that did not correspond to any previously characterized silk composition, while the amino acid composition of dragline silk obtained through forcible silking of black widows was similar to that of orb weavers. Yet, for 10 of the 11 amino acids Casem et al. (1999) studied, including all amino acids constituting more than 1.5% of the silk proteins, *L. hesperus* scaffolding silk and *L. hesperus* dragline silk were more similar to one

another than either was to dragline silk of orb weavers. Thus, it does not appear that the amino acid composition of black widow scaffold silk differs substantially from black widow dragline or orb weaver major ampullate silk. Instead, the similarity in amino acid composition seems to support the conclusion that *L. hesperus* cobweb silk and dragline silk are identical materials. This is also congruent with our finding that the mechanical behavior of sheet/supporting threads and forcibly silked major ampullate fibers from *L. hesperus* were mechanically similar. We therefore feel secure in concluding that the origin of most fibers within the sheet and supporting structure of *L. hesperus* cobwebs is the major ampullate gland.
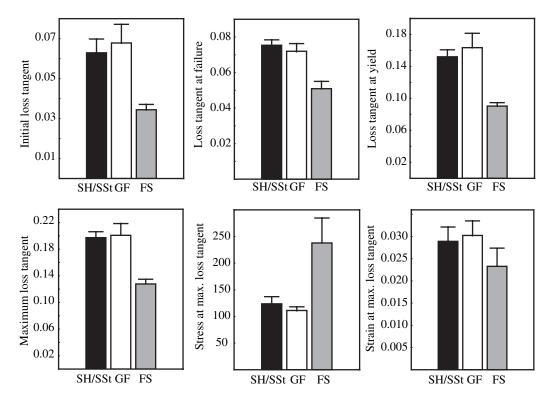
It should be noted that Casem et al. (1999) found that

Fig. 9. Mean (±S.E.M.) dynamic properties for sheet/supporting threads (SH/SSt; $N=12$), gumfooted lines (GF; $N=21$), and forcibly silked major ampullate threads (FS; $N=14$). All properties differed among silks, except strain at max. loss tangent (one-way ANOVAs, $F_{2,35}=5–13$, P at least <0.005). *Post hoc* comparsions of means using Tukey's HSD tests for unequal sample sizes indicated that the performance of the forcibly silked major ampullate fibers was significantly different from sheet/supporting threads and gumfooted lines for all properties except strain at max. loss tangent (P at least <0.05).

solubilized proteins from black widow dragline and scaffolding silk migrated differently on an SDS-PAGE gel. This suggests that perhaps there might be differences that persist through the electrophoresis process in how the major ampullate silk molecules from draglines and scaffolds amalgamate with one another. Alternatively, the different banding patterns may be due to the presence of silk from other glands, such as from the pyriform glands, which are used to affix the network of major ampullate fibers to one another and would have been included with the major ampullate fibers in the scaffold/sheet of the cobweb.

The orb-weaving ancestors of theridiids constructed webs using a framework of major ampullate threads and a capture spiral of flagelliform fibers coated with aggregate glue droplets (Coddington and Levi, 1991; Griswold et al., 1998). Thus, as the adhesive capture element of the cobweb, the sticky gumfooted thread is functionally similar to orb web capture spiral (Blackledge et al., 2005b). However, the glandular origin of the silk used to construct the gumfooted capture threads of cobwebs has been uncertain and hypotheses have included major ampullate, minor ampullate, and flagelliform glands (Benjamin and Zschokke, 2002; Coddington, 1986). We found that sticky gumfooted lines are clearly not mechanically equivalent to flagelliform silk because even the viscid regions of sticky gumfooted threads (Fig. 11) lack the 400% or greater extensibility exhibited by orb weaver capture fibers (Denny, 1976; Köhler and Vollrath, 1995; Opell and Bond, 2001). Other researchers have suggested that gumfooted threads are composed of one thicker pair of major ampullate fibers and a second thinner pair of minor ampullate threads (Benjamin and Zschokke, 2002). We did find that one pair of fibers within the gumfooted thread was always thicker than the other. However, that difference was within the range of variation for black widow major ampullate silk as suggested by scaffolding and forcibly silked fibers (Fig. 3), while the diameter of 12 minor

ampullate fibers that we obtained from *L. hesperus* using the same forcible silking technique described above were all much smaller than either gumfooted fibers or forcibly silked major ampullate fibers (mean ± S.E.M. = 1.1±0.1 µm for minor ampullate fibers compared with Fig. 3). Our mechanical data also suggest that the gumfooted fibers are all composed of major ampullate silk because the dry region of the gumfooted threads was virtually identical to that of the rest of the cobweb. In contrast, the mechanical performance of the 12 minor ampullate fibers that we obtained through forcibly silking was strikingly different. In particular, Young's modulus for minor ampullate fibers (mean ± S.E.M. = 6.3±0.4 GPa) was about 40% lower than that for gumfooted threads and other major ampullate fibers (Table 1), indicating that the crystalline structure of minor ampullate fibers was unlike that of cobweb silks. Finally, there was little difference in the mechanical performance between paired samples of the upper, two fiber, and lower, four fiber, dry regions of the gumfoots (paired *t*-tests, *P*>0.05 for all variables except tensile strength, which was significantly higher for the upper region at *P*<0.05, *N*=15). This suggests that all four threads are spun from the same silk proteins. Therefore, we conclude that gumfooted threads are constructed from major ampullate silk fibers, like the scaffolding support elements of the cobweb (see also Blackledge et al., 2005b).

We found that forcibly silked fibers of major ampullate silk were stiffer and less extensible that naturally spun fibers from
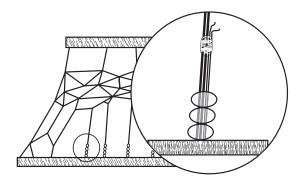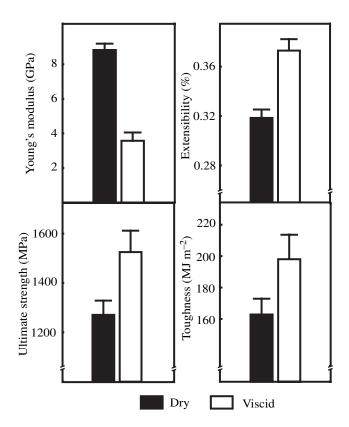

Fig. 10. Gumfooted lines consist of two pairs of silk fibers that are coated with an aggregate silk glue along their lower 5–15 mm. One pair of fibers has a larger diameter and runs continuously from the sheet to the substrate. The second pair of smaller diameter silk fibers is cut by the spiders just above an attachment point to the larger fibers. Thus, the 'foot' of the line consists of four fibers that are viscid (glue covered) along their base and are then dry until the attachment point, while the bulk of the gumfoot is two dry, large diameter fibers.

Fig. 11. Mean (±S.E.M.) mechanical properties of adjacent regions of dry and viscid gumfooted lines (*N*=21).
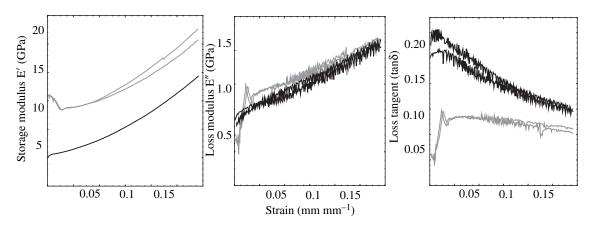
Fig. 12. Dynamic mechanical properties of viscid (black) and dry (gray) portions of the gumfooted lines. Two pairs of samples are shown.

scaffolds and gumfoots. This difference between forcibly silked fibers and native silks has also been seen in orb-weaving spiders (Madsen et al., 1999; Pérez-Rigueiro et al., 2003). There are at least two potential explanations. Anaesthetizing spiders with CO_2 may alter the pH of the bodies of spiders, thereby affecting assembly of silk polymers (Madsen and Vollrath, 2000). A second possible explanation is that spiders can actively control the flow of the silk fiber through the major ampullate spigot using an internal friction brake. With such a mechanism, spiders may increase the amount of stress applied to the fiber during forcible silking, which could enhance the formation of β-sheet crystalline regions and increase the orientation of the amorphous fibers (Ortlepp and Gosline, 2004). This hypothesis is supported in part by our dynamic data. Forcibly silked fibers had a higher storage modulus and a lower loss modulus than native silks. Both of these differences are consistent with an increased orientation of molecules within the fiber.

Dynamic material properties

Spider silk exhibits an extraordinary capacity to dissipate energy, relative to many other materials (Denny, 1976). Table 2 presents comparative data from a variety of natural and synthetic materials. These data were extracted from DMA studies, which were conducted across a range of temperatures and dynamic oscillation frequencies at very low, constant static strains. Because these DMA data are most comparable to the data that we obtained for spider silk during the initial Hookean region, we chose to present the storage modulus and loss tangent at 1% strain. Temperature can greatly influence the dynamic performance of materials such that we present dynamic data from these other studies only at temperatures near 20°C, because that is the temperature at which we tested our spider silk. It is readily apparent from Table 2 that black widow major ampullate spider silk has a storage modulus that is much higher than most other materials. Moreover, the loss tangent for spider silk is approximately an order of magnitude higher than other materials, except for rubber and elastin, both of which have very low dynamic stiffness. Thus, spider silk has a unique combination of high storage modulus and high

loss tangent that results in an immense capacity to dissipate kinetic energy.

The dynamic mechanical behavior of black widow silk is congruent with existing hypotheses about the structure of major ampullate spider silk at the molecular level. Structural studies of major ampullate spider silk suggest that it consists primarily of a matrix of amorphous polypeptide chains with small crystals, formed from β-pleated sheets, embedded within that matrix (Gosline et al., 1999; Xu and Lewis, 1990). Molecular models of major ampullate spider silk suggest that these crystals play an essential role in providing spider silk with its enormous strength by producing thin regions of locally high modulus that crosslink amino acid chains within the amorphous matrix (Termonia, 1994). This locally high modulus ensures that the crystalline β-sheets undergo little extension as silk fibers are strained. Therefore, it is the amorphous region of the fiber in which most conformational changes are expected to take place as silks are stretched (Warwicker, 1960). It is hypothesized that the initial high stiffness of silk fibers during the first 2% of extension (~10 GPa) is caused by the presence of hydrogen (H) bonds that form between polypeptide chains within the amorphous region. The ability of H-bonds to reform accounts for the high elasticity of this Hookean region. After approximately 2% strain, these H-bonds rapidly break thereby greatly increasing the mobility of polypeptide chains within the amorphous region, which produces a rapid decrease in stiffness (i.e. 'yield'). Subsequent to that yield point, the amorphous chains gradually extend until they are aligned with the fiber axis and the covalent bonds within individual silk fibroins ultimately fail. Atomic force microscopy has corroborated this hypothetical increase in orientation of fibrils during fiber extension for *L. hesperus* scaffolding silk (Gould et al., 1999). Throughout fiber extension, the β-sheets are thought never to strain beyond 2–3% such that the covalent bonding between alanine residues that forms those sheets do not break (Termonia, 1994).

Our dynamic data are consistent with this molecular model of silk (Termonia, 1994). We found that the loss tangent rapidly increases during the first 2–3% strain and reaches a maximum

Table 1. *Comparison of the material properties of black widow silk with other spiders*

	Young's modulus (GPa)	Extensibility (%)	Ultimate strength (MPa)	Toughness (MJ m^{-2})	Reference
L. hesperus SH/SSt (*N*=54)	10.7±2.8	0.42±0.12	1069±204	238±72	This study
L. hesperus GF (*N*=47)	9.2±2.2	0.47±0.06	957±194	236±61	This study
L. hesperus FS (*N*=52)	10.4±3.3	0.33±0.06	996±274	194±58	This study
L. hesperus GS	11±1	0.34±0.08	1000±200	–	Lawrence et al. (2004)
L. hesperus SH/SSt (*N*=30)	6±3	0.22±0.05	1100±500	136±83	Moore and Tran (1999)
Argiope trifasciata ORB (*N*=28)	6.9±2.1	0.30±0.10	600±260	90±52	Pérez-Rigueiro et al. (2001)
Araneus diadematus ORB (*N*=6)	1.2±0.9[a]	0.40±0.13	1154±76[a]	194±–	Köhler and Vollrath (1995)
Nephila clavipes ORB	11±5	0.17±0.05	870±350	–	Work (1976) in Lawrence et al. (2004)
Nephila edulis FS (*N*=48)	8.8±1.5	0.39±0.07	1290±160	217±45	Madsen and Vollrath (2000)
Larinioides sclopetarius[b] ORB (*N*=15)	8.6±–[a]	0.24±–	880±–[a]	105.6±–	Denny (1976)

Mean (±S.D.). We have expressed our data normalized to the original lengths and cross-sectional areas of samples (i.e. engineering stress and strain) to allow comparison with published data on *Latrodectus*. SH/SSt, sheet/supporting threads of cobwebs; GF, gumfooted lines of cobwebs; FS, forcibly silked threads; GS, gravity silked threads; ORB, frame and radii of orb webs. [a]Data were published using true stress rather than engineering values. [b]Name has been changed from *Araneus sericatus* since publication.

Table 2. *Comparison of the dynamic mechanical properties of black widow silk with other natural and synthetic materials*

Material	Storage modulus (GPa)	Loss tangent	Source
Spider silk	10	0.1	This study (at 1% strain)
Bone – human	10	0.040	Yamashita et al. (2001)
Wool	5.5	0.06	Freddi et al. (1999)
Wood (various)	2.5–6.0	0.009–0.011	Birkinshaw et al. (1986)
Polycarbonate	2–3	0.013–0.008	Shelby et al. (2001)
Polypropylene	1–1.5	0.084–0.110	Moore et al. (2004)
Natural rubber with carbon black	0.006	0.2	Xie et al. (2004)
Elastin	0.002	0.2	Gosline and French (1979)

Materials are arranged in descending order of storage modulus.

at the yield point (Fig. 8). This was due to an initial drop in storage modulus that was followed by a rapid increase in loss modulus. This decrease in storage modulus is predicted by the breaking of H-bonds during fiber extension within the elastic region, while the increase in loss modulus is consistent with the frictional heat generated as the mobility of the amorphous chains increases during yield. After the yield point, storage modulus increases as amorphous chains begin to align along the axis of extension while loss modulus increases due to frictional forces. The loss tangent then decreases as individual amorphous chains are strained beyond their maxima and the covalent bonds holding those peptide chains together then rupture.

The change in dynamic behavior of gumfooted lines coated with aggregate glue is also consistent with hypothesized molecular models of major ampullate silk. Aggregate glue contains water molecules that hydrate silk fibers (Vollrath and Edmonds, 1989; Vollrath et al., 1990). This hydration disrupts the hydrogen bonding between amorphous chains thereby decreasing the stiffness of hydrated fibers. Disruption of hydrogen bonding is consistent with the reduced storage modulus that we found for viscid gumfoot silk relative to dry gumfoot (Fig. 12). Furthermore, viscid regions of the gumfooted lines lack the steep increase in loss modulus exhibited by dry fibers because the amorphous chains can already move more freely prior to the yield point. This results in a loss tangent that is initially 400% higher for viscid silk than for dry silk (Fig. 12). Subsequently, loss tangent then rapidly converges for the two types of silk after 15–20% as energy absorption is affected primarily by the physical extension of amorphous chains and the permanent breaking of covalent bonds, which is unaffected by hydration.

Broader implications

We found that the material properties of the silk used to construct cobwebs are strikingly similar to those for orb-weaving spiders (Table 1). Recent analysis of silk cDNA and gene sequences has shown that *Latrodectus geometricus*, a widow that is closely related to *L. hesperus* (Garb et al., 2004), has coding sequences for proteins that resemble the two primary constituents of major ampullate silk from orb-weaving spiders (Gatesy et al., 2001). Furthermore, cDNAs generated from *L. hesperus* major ampullate silk glands (Lawrence et al., 2004) show strong congruence with both the *L. geometricus* and orb weaver major ampullate silk cDNAs.

Current phylogenetic hypotheses for relationships within the Araneae suggest that cobweb spiders are derived from orb-weaving spiders (Coddington and Levi, 1991; Griswold et al., 1998). Thus, the simplest explanation as to why orb web and cobweb weaving spiders share mechanical and biochemical similarities in major ampullate silk is because of their common ancestry. But the question then arises as to what could underlie the stabilizing selection that has maintained the silk characteristics of these taxa that are ecologically diverse and last shared a common ancestor >130 million years ago (Penney, 2002; Selden, 1990). There are several potential explanations for this conservation. One possibility is that despite significant differences in web architecture and the physical challenges of capturing pedestrian versus aerial prey, there may be similar selection acting upon the mechanical function of cobweb and orb web silks. Recent empirical studies have shown that the mechanical properties of orb weaver major ampullate silk may be closely tuned to their function as lifelines for spiders as they fall (Garrido et al., 2002; Osaki, 1996). Because all true spiders (suborder Araneomorphae) have major ampullate spigots (Platnick et al., 1991) and typically spin draglines when moving through the environment, this suggests that selection for a functional dragline may have played a greater role in shaping the mechanical properties of major ampullate silk than the demands of capturing prey in silken nets. Future studies should examine the quasistatic and dynamic mechanical properties of major ampullate silk from diverse true spiders to discover the phylogenetic and ecological limits to the similarities that we found between the silks spun by cobweb and orb web-weaving spiders.

Symbols

A	cross-sectional area of fibers
E'	storage modulus
E''	loss modulus
E^*	dynamic stiffness
F	force
L	instantaneous fiber length
L_o	fiber gage length
t	time
$\tan\delta$	loss tangent
δ	phase lag
ε_{tr}	true strain
ε_t	dynamic strain
ε_o	dynamic strain amplitude
σ_o	dynamic stress amplitude
σ_{tr}	true stress
σ_t	dynamic stress
ω	angular frequency

References

Agnarsson, I. (2004). Morphological phylogeny of cobweb spiders and their relatives (Araneae, Araneoidea, Theridiidae). *Zool. J. Linnean Soc.* **141**, 447-626.

Arnedo, M. A., Coddington, J., Agnarsson, I. and Gillespie, R. G. (2004). From a comb to a tree: phylogenetic relationships of the comb-footed spiders (Araneae, Theridiidae) inferred from nuclear and mitochondrial genes. *Mol. Phylogenet. Evol.* **31**, 225-245.

Benjamin, S. P. and Zschokke, S. (2002). Untangling the tangle-web: Web construction behavior of the comb-footed spider *Steatoda triangulosa* and comments on phylogenetic implications (Araneae: Theridiidae). *J. Insect Behav.* **15**, 791-809.

Benjamin, S. P. and Zschokke, S. (2003). Webs of theridiid spiders: construction, structure and evolution. *Biol. J. Linnean Soc.* **78**, 293-305.

Birkinshaw, C., Buggy, M. and Henn, G. G. (1986). Dynamic mechanical analysis of wood. *J. Mat. Sci. Lett.* **5**, 898-900.

Blackledge, T. A., Cardullo, R. A. and Hayashi, C. Y. (2005a). Polarized light microscopy, variability in spider silk diameters, and the mechanical characterization of spider silk. *Invert. Zool.* **124**, 165-173.

Blackledge, T. A., Summers, A. P. and Hayashi, C. Y. (2005b). Gumfooted lines in black widow cobwebs and the mechanical properties of spider capture silk. *Zoology* **108**, 41-46.

Casem, M. L., Turner, D. and Houchin, K. (1999). Protein and amino acid composition of silks from the cob weaver, *Latrodectus hesperus* (black widow). *Int. J. Biol. Macromol.* **24**, 103-108.

Coddington, J. A. (1986). The monophyletic origin of the orb web. In *Spiders: Webs, Behavior and Evolution* (ed. W. A. Shear), pp. 319-363. Stanford, USA: Stanford University Press.

Coddington, J. A. (1990). Cladistics and spider classification Araneomorph phylogeny and the monophyly of orb-weavers (Araneae: Araneomorphae: Orbiculariae). *Acta Zool. Fennica* **190**, 75-88.

Coddington, J. A. and Levi, H. W. (1991). Systematics and evolution of spiders (Araneae). *Annu. Rev. Ecol. Systematics* **22**, 565-592.

Denny, M. (1976). Physical properties of spider silks and their role in design of orb-webs. *J. Exp. Biol.* **65**, 483-506.

Freddi, G., Tsukada, M. and Shiozaki, H. (1999). Chemical modifications of wool fibers with acid anhydrides. *J. Appl. Polymer Sci.* **71**, 1573-1579.

Garb, J. E., Gonzalez, A. and Gillespie, R. G. (2004). The black widow spider genus *Latrodectus* (Araneae: Theridiidae): phylogeny, biogeography, and invasion history. *Mol. Phylogenet. Evol.* **31**, 1127-1142.

Garrido, M. A., Elices, M., Viney, C. and Pérez-Rigueiro, J. (2002). Active control of spider silk strength: comparison of drag line spun on vertical and horizontal surfaces. *Polymer* **43**, 1537-1540.

Gatesy, J., Hayashi, C., Motriuk, D., Woods, J. and Lewis, R. (2001). Extreme diversity, conservation and convergence of spider silk fibroin sequences. *Science* **291**, 2603-2605.

Gosline, J. M. and French, C. J. (1979). Dynamic mechanical properties of elastin. *Biopolymers* **18**, 2091-2103.

Gosline, J. M., Demont, M. E. and Denny, M. W. (1986). The structure and properties of spider silk. *Endeavour* **10**, 37-43.

Gosline, J. M., Guerette, P. A., Ortlepp, C. S. and Savage, K. N. (1999). The mechanical design of spider silks: from fibroin sequence to mechanical function. *J. Exp. Biol.* **202**, 3295-3303.

Gould, S. A. C., Tran, K. T., Spagna, J. C., Moore, A. M. F. and Shulman, J. B. (1999). Short and long range order of the morphology of silk from *Latrodectus hesperus* (Black Widow) as characterized by atomic force microscopy. *Int. J. Biol. Macromol.* **24**, 151-157.

Griswold, C. E., Coddington, J. A., Hormiga, G. and Scharff, N. (1998). Phylogeny of the orb-web building spiders (Araneae, Orbiculariae: Deinopoidea, Araneoidea). *Zool. J. Linnean Soc.* **123**, 1-99.

Hodar, J. A. and Sanchez-Pinero, F. (2002). Feeding habits of the black widow spider *Latrodectus lilianae* (Araneae: Theridiidae) in an arid zone of south-east Spain. *J. Zool.* **257**, 101-109.

Köhler, T. and Vollrath, F. (1995). Thread biomechanics in the two orb-

weaving spiders *Araneus diadematus* (Araneae, Araneidae) and *Uloborus walckenaerius* (Araneae, Uloboridae). *J. Exp. Zool.* **271**, 1-17.

Lawrence, B. A., Vierra, C. A. and Moore, A. M. F. (2004). Molecular and mechanical properties of major ampullate silk of the black widow spider, *Latrodectus hesperus*. *Biomacromolecules* **5**, 689-695.

Madsen, B. and Vollrath, F. (2000). Mechanics and morphology of silk drawn from anesthetized spiders. *Naturwissenschaften* **87**, 148-153.

Madsen, B., Shao, Z. Z. and Vollrath, F. (1999). Variability in the mechanical properties of spider silks on three levels: interspecific, intraspecific and intraindividual. *Int. J. Biol. Macromol.* **24**, 301-306.

Moore, A. M. F. and Tran, K. (1999). Material properties of cobweb silk from the black widow spider *Latrodectus hesperus*. *Int. J. Biol. Macromol.* **24**, 277-282.

Moore, E. M., Ortiz, D. L., Marla, V. T., Shambaugh, R. L. and Grady, B. P. (2004). Enhancing the strength of polylpropylene fibers with carbon nanotubes. *J. Appl. Polymer Sci.* **93**, 2926-2933.

Opell, B. D. and Bond, J. E. (2001). Changes in the mechanical properties of capture threads and the evolution of modern orb-weaving spiders. *Evol. Ecol. Res.* **3**, 567-581.

Ortlepp, C. S. and Gosline, J. M. (2004). Consequences of forced silking. *Biomacromolecules* **5**, 727-731.

Osaki, S. (1996). Spider silk as mechanical lifeline. *Nature* **384**, 419.

Penney, D. (2002). Spiders in upper cretaceous amber from New Jersey (Arthropoda: Araneae). *Palaeontology* **45**, 709-724.

Pérez-Rigueiro, J., Elices, M., Llorca, J. and Viney, C. (2001). Tensile properties of *Argiope trifasciata* drag line silk obtained from the spider's web. *J. Appl. Polymer Sci.* **82**, 2245-2251.

Pérez-Rigueiro, J., Elices, M. and Guinea, G. V. (2003). Controlled supercontraction tailors the tensile behaviour of spider silk. *Polymer* **44**, 3733-3736.

Platnick, N. I., Coddington, J. A., Forster, R. R. and Griswold, C. E. (1991). Spinneret morphology and the phylogeny of haplogyne spiders (Araneae, Araneomorphae). *Am. Museum Novitates*, **3016**, 1-73.

Selden, P. A. (1990). Lower Cretaceous spiders from the Sierra de Montesch, north-east Spain. *Palaeontology* **33**, 257-285.

Shelby, M. D., Hill, A. J., Burgar, M. I. and Wilkes, G. L. (2001). The effects of molecular orientation on the physical aging and mobility of polycarbonate – solid state NMR and dynamic mechanical analysis. *J. Polymer Sci. B Polymer Phys.* **39**, 32-46.

Termonia, Y. (1994). Molecular modeling of spider silk elasticity. *Macromolecules* **27**, 7378-7381.

Vollrath, F. and Edmonds, D. T. (1989). Modulation of the mechanical properties of spider silk by coating with water. *Nature* **340**, 305-307.

Vollrath, F., Fairbrother, W. J., Williams, R. J. P., Tillinghast, E. K., Bernstein, D. T., Gallagher, K. S. and Townley, M. A. (1990). Compounds in the droplets of the orb spiders viscid spiral. *Nature* **345**, 526-528.

Warwicker, S. O. J. (1960). Comparative studies of fibroins II. The crystal structure of various fibroins. *J. Mol. Biol.* **2**, 350-362.

Work, R. W. (1976). Force-elongation behavior of web fibers and silks forcibly obtained from orb-web-spinning spiders. *Textile Res. J.* **46**, 485-492.

Yamashita, J. l., Furman, B. R., Rawls, H. R., Wang, X. and Agrawal, C. M. (2001). The use of dynamic mechanical analysis to assess the viscoelastic properties of human cortical bone. *J. Biomed. Mat. Res.* **58**, 47-53.

Xie, Z., Wei, Y. T., Liu, Y. and Du, X. (2004). Dynamic mechanical properties of aged filled rubbers. *J. Macromolec. Sci. B Phys.* **43**, 805-817.

Xu, M. and Lewis, R. V. (1990). Structure of a protein superfiber–spider dragline silk. *Proc. Natl. Acad. Sci USA* **87**, 7120-7124.